The BH4 domain of Bcl-X$_L$ rescues astrocyte degeneration in amyotrophic lateral sclerosis by modulating intracellular calcium signals

Francesca Martorana[1,†], Liliana Brambilla[1,†], Chiara F. Valori[2,†,‡], Chiara Bergamaschi[1], Chiara Roncoroni[2], Eleonora Aronica[3], Andrea Volterra[4], Paola Bezzi[4] and Daniela Rossi[1,*]

[1]Laboratory for Research on Neurodegenerative Disorders, IRCCS Fondazione Salvatore Maugeri, 27100 Pavia, Italy, [2]Center of Excellence on Neurodegenerative Diseases, Department of Pharmacological Sciences, University of Milan, 20133 Milan, Italy, [3]Department of Neuropathology, Academisch Medisch Centrum, 1105 AZ Amsterdam, The Netherlands and [4]Department of Cell Biology and Morphology, University of Lausanne, 1005 Lausanne, Switzerland

Collective evidence indicates that motor neuron degeneration in amyotrophic lateral sclerosis (ALS) is non-cell-autonomous and requires the interaction with the neighboring astrocytes. Recently, we reported that a subpopulation of spinal cord astrocytes degenerates in the microenvironment of motor neurons in the hSOD1^{G93A} mouse model of ALS. Mechanistic studies *in vitro* identified a role for the excitatory amino acid glutamate in the gliodegenerative process via the activation of its inositol 1,4,5-triphosphate (IP$_3$)-generating metabotropic receptor 5 (mGluR5). Since non-physiological formation of IP$_3$ can prompt IP$_3$ receptor (IP$_3$R)-mediated Ca^{2+} release from the intracellular stores and trigger various forms of cell death, here we investigated the intracellular Ca^{2+} signaling that occurs downstream of mGluR5 in hSOD1^{G93A}-expressing astrocytes. Contrary to wild-type cells, stimulation of mGluR5 causes aberrant and persistent elevations of intracellular Ca^{2+} concentrations ([Ca^{2+}]$_i$) in the absence of spontaneous oscillations. The interaction of IP$_3$Rs with the anti-apoptotic protein Bcl-X$_L$ was previously described to prevent cell death by modulating intracellular Ca^{2+} signals. In mutant SOD1-expressing astrocytes, we found that the sole BH4 domain of Bcl-X$_L$, fused to the protein transduction domain of the HIV-1 TAT protein (TAT-BH4), is sufficient to restore sustained Ca^{2+} oscillations and cell death resistance. Furthermore, chronic treatment of hSOD1^{G93A} mice with the TAT-BH4 peptide reduces focal degeneration of astrocytes, slightly delays the onset of the disease and improves both motor performance and animal lifespan. Our results point at TAT-BH4 as a novel glioprotective agent with a therapeutic potential for ALS.

INTRODUCTION

In the adult nervous system, the major glial cell type is represented by the astrocytes. These cells fulfill several homeostatic functions that collectively contribute to maintain the optimal microenvironment for neuronal function and survival (1,2). In addition, astrocytes can sense neuronal activity by a large repertoire of neurotransmitter receptors located in their plasma membrane (3) and, in turn, they can respond to neurons by Ca^{2+}-dependent release of gliotransmitters (4,5). The multiplicity and complexity of these activities clearly indicate that the correct performance of the astrocytes is crucial for the physiological functioning of the nervous system and its derangement may affect neuronal activity and contribute to neurodegeneration.

A growing number of recent observations suggests that, in amyotrophic lateral sclerosis (ALS), a complex pathological interplay subsists between motor neurons and the neighboring

*To whom correspondence should be addressed at: Laboratory for Research on Neurodegenerative Disorders, IRCCS Fondazione Salvatore Maugeri, Via Maugeri 10, 27100 Pavia, Italy. Tel: +39 0382592064; Fax: +39 0382592094; Email: daniela.rossi@fsm.it
†These authors contributed equally to this work.
‡Present address: Institute of Neuropathology, Schmelzbergstrasse 12, 8091 Zurich, Switzerland.

glial cells, particularly astrocytes (6–12). Astroglial cells were described to cause damage to motor neurons directly by releasing toxic factors, but also indirectly via the loss of their physiological functions (10,11,13–23). Within this framework, we and others reported that a subset of astrocytes, positioned in the microenvironment of motor neurons, undergoes degeneration in the spinal cord of transgenic mice over-expressing the G93A form of mutant human superoxide dismutase 1 (hSOD1^{G93A}) (24,25). This phenomenon occurs prior to symptom onset and is mediated by the excitatory amino acid glutamate via the activation of its inositol 1,4,5-triphosphate (IP$_3$)-producing metabotropic receptor type-5 (mGluR5) (25). The physiological production of IP$_3$ under the stimulation of cell-surface receptors, such as mGluR5, normally triggers the release of Ca^{2+} from the endoplasmic reticulum (ER) by opening the IP$_3$ receptor (IP$_3$R) channels. Such Ca^{2+} plays a role in modulating a variety of cellular responses that are fundamental for cell function and survival (26). However, Ca^{2+} released under non-physiological conditions can activate different pathways of cell death (27–31). Importantly, the anti-apoptotic Bcl-2 family members, particularly Bcl-2 and Bcl-X$_L$, were reported to confer cell death protection by altering the Ca^{2+} permeability of the IP$_3$R channels (29,31–38). The anti-apoptotic activity of these proteins has been mostly ascribed to their homology domain 4 (BH4), and the one from Bcl-X$_L$ appears to be more efficient than that of Bcl-2 (39–41).

As a protective role for the Bcl-2 family proteins has been clearly identified in the mechanisms of cell death triggered by ALS-linked mutant SOD1s (42–48), here we tested the impact on astrocyte physiology and survival of a biologically active peptide consisting of the BH4 domain of Bcl-X$_L$ fused to the protein transduction domain of the human immunodeficiency virus (HIV) TAT protein (TAT-BH4). We report that although mGluR5-driven degeneration of ALS astrocytes is coupled to aberrant intracellular Ca^{2+} handling, the treatment with TAT-BH4 affords cell death resistance by enhancing pro-survival Ca^{2+} oscillations. Furthermore, chronic administration of TAT-BH4 *in vivo*, to hSOD1^{G93A} transgenic mice, reduces degeneration of spinal cord astrocytes, slightly postpones the appearance of ALS symptoms and improves both motor performance and survival.

RESULTS

Aberrant expression of mGluR5 in ALS tissues

A degenerative process of the astrocytes that spatially and temporally correlates with the progression of ALS disease was previously identified in the spinal cord of hSOD1^{G93A} mice (25). Degenerating astroglial cells were morphologically characterized by an unusually thick and spheroidal cap of glial fibrillary acidic protein (GFAP) (Fig. 1A, hSOD1^{G93A}, 100 days), which was associated with rare GFAP-positive processes and resulted immunopositive for the active caspase-3 (25). Neuropathological analyses of autoptic tissues from patients affected by sporadic ALS confirmed that these unusual GFAP- and active caspase-3-positive cellular profiles are present in the neighborhood of motor neurons also in the ventral horns of the spinal cord from sALS cases (Fig. 1B

and Supplementary Material, Fig. S1). Because a role for mGluR5 was originally identified in the gliodegenerative process *in vitro* (25), we next investigated the expression of the receptor messenger RNA (mRNA) *in vivo*, in the spinal cord of hSOD1^{G93A} ALS mice and wild-type control animals, at different ages during disease progression. Quantitative reverse transcription-polymerase chain reaction (qRT-PCR) analysis revealed that, in wild-type mice, mGluR5 mRNA levels remain fairly constant throughout life (Supplementary Material, Fig. S2A). In contrast, at the pre-symptomatic age of 30 days, the transcripts of the receptor result up-regulated in hSOD1^{G93A} mice when compared with age-matched wild-type animals. Yet, their levels significantly decrease at the time of disease onset, i.e. about 100 days of age, when the degree of expression becomes comparable with that in wild-type mice (Supplementary Material, Fig. S2A).

The expression and cellular distribution of the mGluR5 protein was subsequently explored *in situ* in mGluR5-immunolabeled spinal cord sections from hSOD1^{G93A} and wild-type animals. In both instances, we found that mGluR5 shows the typical punctuate staining of receptor clusters throughout lumbar spinal cord sections, in both neuronal as well as glial cells (Fig. 1A and Supplementary Material, Fig. S2B). However, quantitative analysis of mGluR5-immunofluorescent puncta confirmed a generally enhanced expression of the receptor in 30-day-old hSOD1^{G93A} mice when compared with wild-type animals (Supplementary Material, Fig. S2C). Because at this phase of the disease, the degree of expression of the astrocytic and microglial markers, GFAP and CD11b, was similar in the two genotypes (GFAP or CD11b expression levels in wild-type mouse spinal cord were set as 100%; expression levels in 30-day-old hSOD1^{G93A} mouse spinal cord: GFAP: 75 ± 13% versus wild-type, $P = 0.27$, unpaired t-test; CD11b: 102 ± 15% versus wild-type, $P = 0.12$, unpaired t-test, $n = 6$ fields from three mice), we infer that the increase in mGluR5 levels is independent on hyperproliferation of reactive glia. Rather, it is a consequence of the presence of mutant SOD1 in the different cell types. Interestingly, immunohistochemical analyses of hSOD1^{G93A} spinal cords, taken at the time of disease onset, confirmed that the expression of mGluR5 was quantitatively comparable with wild-type spinal cords, but significantly lower than that in 30-day-old ALS mice (Supplementary Material, Fig. S2C). This decrease in the amount of mGluR5 cannot be fully ascribed to motor neuron loss (Fig. 7E), as we observed a substantial reduction in the expression of the receptor (−27.8 ± 2.3%, $n = 9$ fields from three mice) also in regions of the spinal cord where the motor cells are still alive. Noteworthy, at this stage of the disease, degenerating astrocytes were largely represented and maintained a stronger immunoreactivity for mGluR5 when compared with the neighboring cells. This profile was determined by enhanced and closely adjacent mGluR5-positive puncta (Fig. 1A, hSOD1^{G93A}, 100 days). In keeping with these observations, we found a similar pattern of mGluR5 expression also in autoptic sALS spinal cords (Fig. 1B). The fact that mGluR5 is over-expressed in the spinal cord of hSOD1^{G93A} mice at the pre-symptomatic stage of the disease, but not at the time of disease onset strongly suggests that this receptor plays a
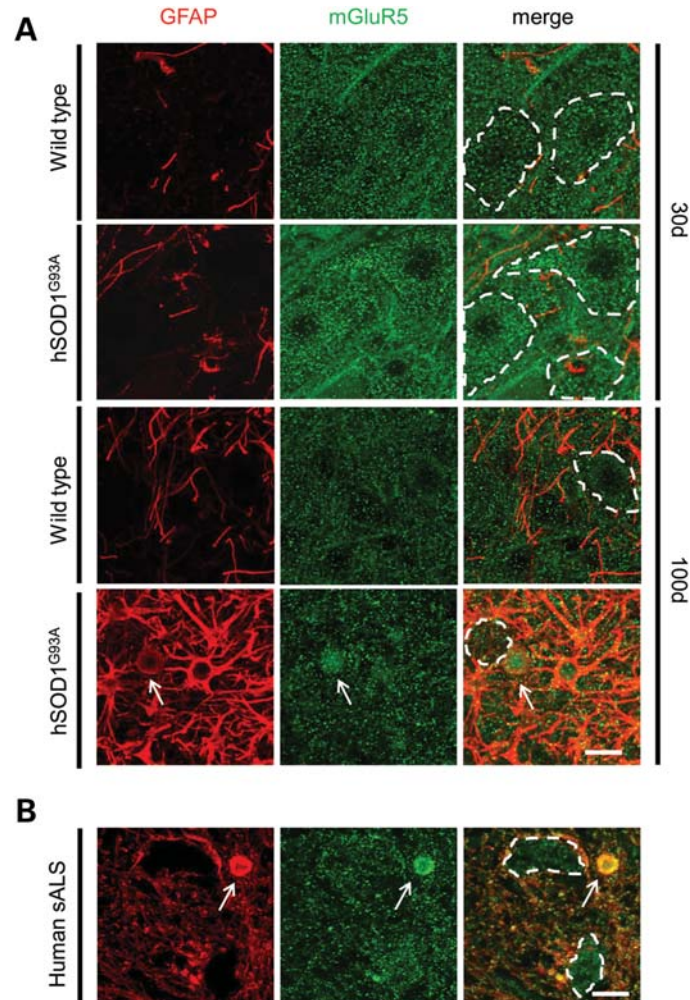
Figure 1. Distribution of mGluR5 in the spinal cord of hSOD1^{G93A} mice and sporadic ALS patients. (**A**) Representative images of lumbar spinal cord sections from 30- (30d) and 100-day-old (100d) wild-type and hSOD1^{G93A} mice. Sections were double-immunostained for GFAP (red) and mGluR5 (green) to visualize astrocytic cytoskeleton and metabotropic glutamate receptor clusters, respectively. (**B**) Typical images of human post-mortem ALS spinal cord sections double-immunolabeled with antibodies against GFAP (red), to mark the astrocytic cytoskeleton, and mGluR5 (green), to visualize the metabotropic glutamate receptor puncta. (A, B) Dotted lines outline motor neuronal cell bodies. Scale bar, 20 μm.

crucial role in ALS progression by acting at the early stages of the disease. Its persistent, enhanced expression in degenerating astrocytes then indicates that mGluR5 may be involved in the gliodegenerative process *in vivo*.

Altered mGluR5-mediated intracellular calcium ([Ca^{2+}]$_i$) signaling in hSOD1^{G93A}-expressing astrocytes is coupled to cell death

To determine whether the global over-expression of mGluR5 identified in the spinal cord of young ALS mice was reflected on astrocytes, we next switched to studies in cell culture. First, we quantified the levels of the receptor mRNA in primary astrocytes deriving from the spinal cord of newborn hSOD1^{G93A} and wild-type animals. qRT-PCR analysis indicated that hSOD1^{G93A}-expressing astrocytes show a 2.6-fold increase in the amount of mGluR5 transcripts when compared with wild-type sister cultures (Supplementary Material, Fig. S3). The mGluR5 Ca^{2+}-signaling was then studied by

single-cell Fluo4 imaging of the [Ca^{2+}]$_i$ changes induced by (RS)-3,5-dihydroxyphenylglycine (DHPG), a selective agonist of the group I metabotropic glutamate receptors (mGluRs). Consistent with previous reports (49,50), we found that the majority of wild-type astrocytes (about 68%, Fig. 2A and C) responded to the local application of 100 μM DHPG with a single [Ca^{2+}]$_i$ transient followed by sustained [Ca^{2+}]$_i$ oscillations (Fig. 2A and C) (49,50). In hSOD1^{G93A}-expressing astrocytes, the [Ca^{2+}]$_i$ signaling features were completely different; almost all astrocytes challenged with DHPG (about 99%) displayed a decreased initial [Ca^{2+}]$_i$ transient (−63% of $\Delta F/F_0$ with respect to wild-type cells, Fig. 2B and C), followed by a secondary long-lasting rise in cytosolic [Ca^{2+}]$_i$ reaching the plateau level in about 10 min. The amplitude of the [Ca^{2+}]$_i$ plateau was slightly heterogeneous, ranging from 0.25 to 0.8 $\Delta F/F_0$, and this pattern was associated to the lack of oscillatory [Ca^{2+}]$_i$ signals (Fig. 2B and C). Next, we investigated the mechanisms responsible for this atypical DHPG-induced [Ca^{2+}]$_i$ rise in
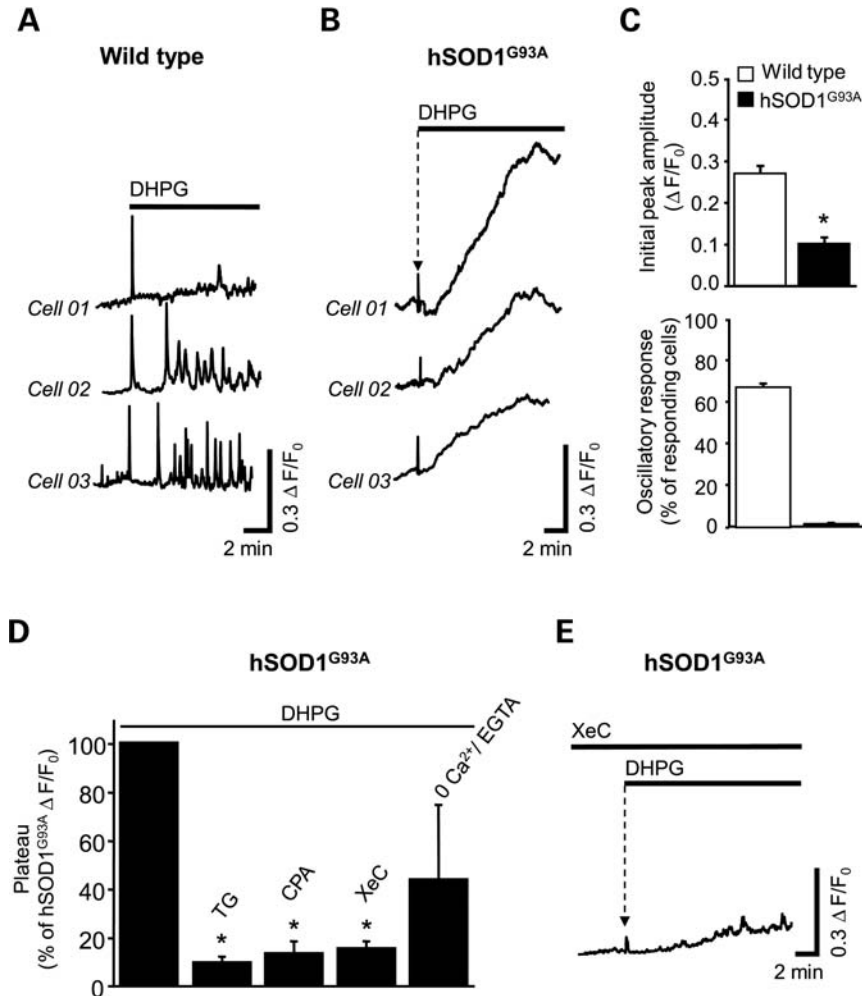
Figure 2. Impact of hSOD1[G93A] on DHPG-induced $[Ca^{2+}]_i$ signaling in astrocytes. (**A**–**C**) Local application of the group I mGluR agonist DHPG induced $[Ca^{2+}]_i$ signaling in wild-type and hSOD1[G93A]-cultured astrocytes. (A) Typical single-cell $[Ca^{2+}]_i$ transients obtained in response to 100 μM DHPG in three wild-type astrocytes. Note that the majority of cells (67.7 ± 1.23%; $n = 93$ cells analyzed; $n = 7$ experiments) responded with a single $[Ca^{2+}]_i$ transient ($\Delta F/F_0$: 0.27 ± 0.18) followed by sustained $[Ca^{2+}]_i$ oscillations (average frequency: 17 ± 2.5 mHz). (B) As in (A) but in hSOD1[G93A] astrocytes. Note that contrary to wild-type astrocytes, the majority of hSOD1[G93A]-expressing cells (99 ± 2.5%; $n = 84$ cells analyzed; $n = 6$ experiments) responded to DHPG with a reduced single $[Ca^{2+}]_i$ transient (-63%; $\Delta F/F_0$: 0.1 ± 0.08) followed by an abnormal long-lasting calcium rise that reaches the plateau in about 10 min ($\Delta F/F_0$: 0.55 ± 0.3). (C) Summary (mean ± s.e.m.) of >50 cells in multiple trials representing peak amplitude of initial DHPG-evoked $[Ca^{2+}]_i$ transient (expressed as $\Delta F/F_0$) (top) and percentage of cells responding with oscillations (bottom) (*$P < 0.001$, unpaired t-test versus wild-type cells). (**D**) Summary (mean ± s.e.m.) of >30 cells in multiple trials representing the $[Ca^{2+}]_i$ plateau obtained in hSOD1[G93A] astrocytes upon treatment with 100 μM DHPG in the absence or presence of thapsigargin (1 μM, TG), cyclopiazonic acid (10 μM, CPA), xestospongin C (1 μM, XeC) or 0 Ca^{2+}/EGTA (5 mM). Data are expressed as percentage of $\Delta F/F_0$ calculated in DHPG-treated hSOD1[G93A] cells (*$P < 0.01$, paired t-test versus hSOD1[G93A]). (**E**) Typical single-cell $[Ca^{2+}]_i$ transients obtained in one DHPG-treated hSOD1[G93A] astrocyte in the presence of XeC. Note that the majority of cells treated with XeC (95 ± 3.5%; $n = 45$ cells analyzed; $n = 8$ experiments) responded with a reduced single $[Ca^{2+}]_i$ transient ($\Delta F/F_0$: 0.050 ± 0.007) followed by a slight, but not significant, increase in calcium ($\Delta F/F_0$: 0.078 ± 0.01).

ALS astrocytes. We reasoned that the increase in cytosolic Ca^{2+} could be caused by stimulated Ca^{2+} release from IP_3-sensitive intracellular Ca^{2+} stores or by increased influx of extracellular Ca^{2+}.

As it is well known that group I mGluRs are typically coupled to IP_3 formation, and this activates IP_3R-mediated $[Ca^{2+}]_i$ signaling, we first explored the involvement of both the ER Ca^{2+} stores and the IP_3Rs. We found that pre-treatment with thapsigargin (TG, 1 μM) or cyclopiazonic acid (CPA, 10 μM), two irreversible ER Ca^{2+}-ATPase inhibitors (51,52), almost completely prevented the DHPG-induced $[Ca^{2+}]_i$ increase in mutant SOD1-expressing cells (Fig. 2D) (53).

Similarly, application of xestospongin C (XeC, 1 μM), a specific inhibitor of the IP_3 receptors (54), reduced the amplitude of the initial peak to about 20% of the control level and significantly decreased the following persistent rise in cytosolic Ca^{2+} (-85% of $\Delta F/F_0$ with respect to hSOD1[G93A] cells, Fig. 2D and E). The role of extracellular Ca^{2+} influx was subsequently examined by stimulating hSOD1[G93A] spinal cord astrocytes with DHPG in 0 Ca^{2+} and in the presence of the Ca^{2+} chelator ethyleneglycol-bis(β-aminoethyl)-N,N,N′,N′-tetraacetic acid (EGTA, 5 mM). Consistent with the experiments performed in the presence of Ca^{2+}, DHPG triggered an initial Ca^{2+} transient ($\Delta F/F_0$: 0.092 ± 0.04) followed by
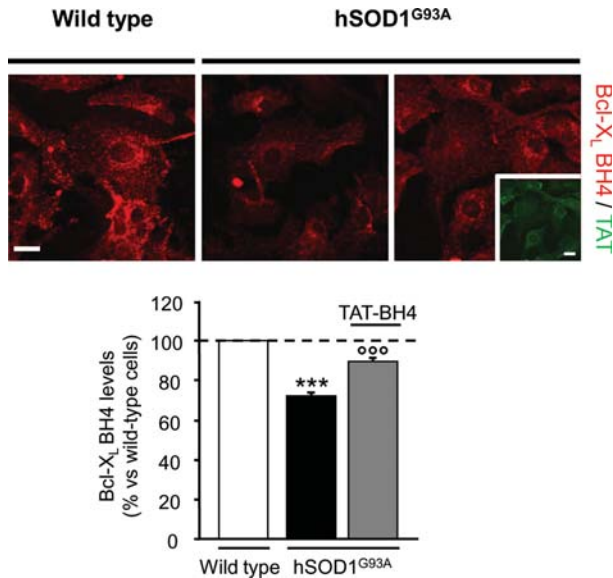
Figure 3. Treatment with TAT-BH4 restores normal levels of Bcl-X$_L$ BH4 in hSOD1^{G93A} spinal astrocytes. Astrocyte cultures from the spinal cord of wild-type or hSOD1^{G93A} mice were treated in the absence or presence of 0.5 μM TAT-BH4 and immunolabeled for Bcl-X$_L$ (red) and TAT (green) proteins. An antibody that recognizes the amino-terminal BH4 domain of Bcl-X$_L$ (57) and, thus, reacts with both the endogenous full-length protein and the internalized TAT-BH4 peptide, was used to visualize the global levels of BH4 within the cells. Inset shows TAT immunoreactivity in hSOD1^{G93A} cells treated with the peptide. Scale bars, 20 μm. Histograms show the levels of Bcl-X$_L$ BH4 in the different experimental conditions, as determined by immunofluorescence quantification. Data (mean ± s.e.m.) are expressed as percentage of Bcl-X$_L$ BH4 levels in wild-type astrocytes ($n = 50$ cells for each experimental group) (***$P < 0.0001$ versus wild-type astrocytes and °°°$P < 0.0001$ versus hSOD1^{G93A}-expressing astrocytes, one-way ANOVA followed by Bonferroni *post-hoc* test).

a long-lasting rise in [Ca^{2+}]$_i$ reaching a plateau level ($\Delta F/F_0$: 0.23 ± 0.16, Fig. 2D) in several minutes. Remarkably, no significant differences were found between the conditions with and without extracellular calcium (Fig. 2D). This suggests that the DHPG-mediated [Ca^{2+}]$_i$ plateau observed in hSOD1^{G93A} spinal cord astrocytes is not due to the influx of extracellular Ca^{2+}, but it is mostly caused by the activation of the IP$_3$ receptors and the release of Ca^{2+} from the internal stores.

Considerable evidence suggests that the function of the ER is intimately connected with that of mitochondria. Thus, during normal signaling, there is a continuous flow of Ca^{2+} between the two organelles, which is relevant for the mitochondrial metabolic activity. However, alterations in Ca^{2+} homeostatic mechanisms that result in massive and/or prolonged mitochondrial [Ca^{2+}]$_i$ overload can cause the release of cytochrome c, located between the inner and the outer mitochondrial membranes. This event can lead to the activation of cell death effector caspases (30,31). On the basis of these considerations, we postulated that the unusual efflux of intracellular Ca^{2+} detected in the mutant SOD1-expressing cells, in combination with the loss of IP$_3$R-dependent [Ca^{2+}]$_i$ oscillations, may underlie degeneration of ALS astrocytes (31). In agreement with this hypothesis, we confirmed that the same concentration of DHPG triggers the release of cytochrome c

from mitochondria (Fig. 5A). This event is associated with delayed (24 h) caspase-3 activation and nuclear condensation in a subset of mutant SOD1-expressing astrocytes (Fig. 5B). Because mGluR5, but not the closely related mGluR1 (55), is expressed in cultured astrocytes, we conclude that the effects elicited by DHPG in ALS astroglial cells can be ascribed to mGluR5 activation.

The BH4 domain of Bcl-X$_L$ restores [Ca^{2+}]$_i$ oscillations in hSOD1^{G93A}-expressing astrocytes

Several lines of evidence indicate that the Bcl-2 homologs are important regulators of cell death mechanisms, and this has been attributed, at least in part, to their ability to modulate ER Ca^{2+} signals (29–31,38). Notably, Bcl-X$_L$ was reported to exert its full anti-apoptotic effects by directly binding to the IP$_3$Rs. This interaction was shown to sensitize cells to low concentrations of IP$_3$ and enhance spontaneous [Ca^{2+}]$_i$ oscillations, an event that has been correlated with increased cell death resistance (36,37). On the basis of this, we next investigated the expression of Bcl-X$_L$ in cultured astrocytes by immunocytochemistry. Immunofluorescence quantification revealed that the levels of Bcl-X$_L$ were significantly reduced to ~78% in astrocytes harboring mutant SOD1 when compared with wild-type cells (Fig. 3). As the BH4 domain of Bcl-X$_L$ importantly contributes to cell death suppression (35,39–41), we then examined whether a fusion peptide, in which BH4 is conjugated with the cell-penetrating TAT peptide from the HIV-1 virus (TAT-BH4, Supplementary Material, Fig. S4A) (56), was transduced into primary astrocytes, and we studied its stability inside the cells over time. Astroglial cells in culture were thus incubated with either unconjugated or 5(6)-carboxyfluorescein (FAM)-conjugated TAT-BH4 (TAT-BH4-FAM, 0.5 μM, 30 min, Supplementary Material, Fig. S4B). Cells were subsequently washed and either immediately fixed or maintained in culture for 24 h and then fixed, according to the timing of our toxicity experiments (25). The presence of TAT-BH4-FAM into nearly 100% of astrocytes was confirmed by fluorescence microscopy. Furthermore, significant levels of the transduced fluorescent marker persisted in the astrocytes even 24 h after the removal of the peptide from the cell culture media (Supplementary Material, Fig. S4B). Noteworthy, analysis of intracellular BH4 levels, using an antibody that reacts with both the endogenous full-length Bcl-X$_L$ protein and the internalized TAT-BH4 peptide (57), revealed that the treatment with TAT-BH4 restored 94% of Bcl-X$_L$ BH4 levels in mutant SOD1-expressing astrocytes (Fig. 3).

The efficacy of TAT-BH4 in regulating the [Ca^{2+}]$_i$ signaling was then tested in the mutant cells. Calcium imaging experiments were first carried out by challenging Fluo4-loaded wild-type and hSOD1^{G93A}-expressing astrocytes with TAT-BH4 (0.5 μM, 30 min). To our surprise, we found that the local application of TAT-conjugated BH4 caused an immediate [Ca^{2+}]$_i$ rise and restored sustained [Ca^{2+}]$_i$ oscillations in hSOD1^{G93A}-expressing astrocytes (Fig. 4A). These oscillations were strongly inhibited in the presence of agents that either deplete the intracellular Ca^{2+} stores (TG, $-94.5 \pm 3.9\%$ of oscillatory responding cells; $n = 50$ cells analyzed; $n = 8$ experiments) or inhibit the IP$_3$Rs (XeC, $-92.5 \pm$
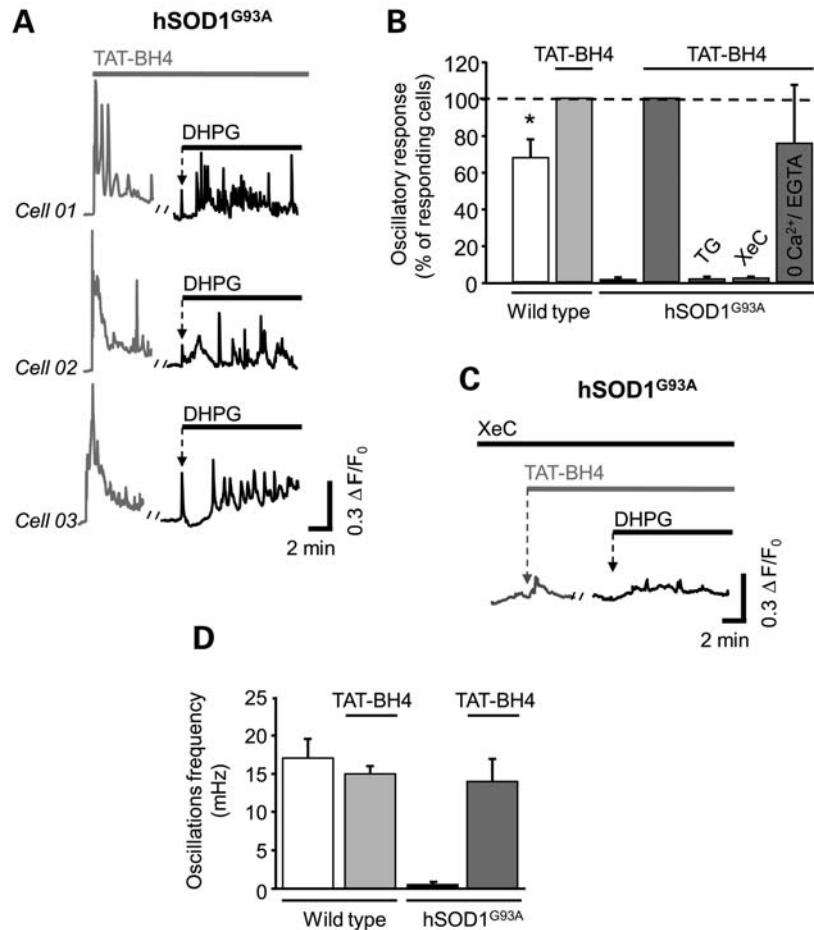
Figure 4. The TAT-BH4 peptide restores spontaneous and DHPG-evoked $[Ca^{2+}]_i$ signaling in hSOD1^{G93A}-expressing astrocytes. (**A**) Representative single-cell $[Ca^{2+}]_i$ transients obtained in three hSOD1^{G93A}-expressing astrocytes treated with TAT-BH4 peptide (0.5 μM; grey traces) for 30 min before the local application of DHPG (100 μM; black traces). Note that in the presence of TAT-BH4 in 100% hSOD1^{G93A}-expressing astrocytes ($n = 90$ cells analyzed; $n = 8$ experiments), DHPG-evoked $[Ca^{2+}]_i$ transients show a pattern similar to that obtained in wild-type astrocytes (Fig. 2A): black traces show a single $[Ca^{2+}]_i$ transient followed by sustained $[Ca^{2+}]_i$ oscillations (average frequency: 14 ± 3.1 mHz). (**B**) Summary (mean $\pm$ s.e.m.) of >40 cells in multiple trials representing the percentage of cells responding with oscillations per each genotype and treatment (thapsigargin 1 μM, TG; xestospongin C 1 μM, XeC; 0 Ca^{2+}/EGTA 5 mM). Note that TG and XeC, but not 0 Ca^{2+}/EGTA, strongly inhibited the oscillatory response induced by DHPG in the majority of TAT-BH4-treated hSOD1^{G93A}-expressing astrocytes (*$P < 0.01$ versus TAT-BH4 in wild-type and TAT-BH4 in hSOD1^{G93A}, two-way ANOVA followed by Bonferroni *post-hoc* test). (**C**) Typical single-cell $[Ca^{2+}]_i$ transients obtained in response to TAT-BH4 (0.5 μM) and DHPG (100 μM) in one hSOD1^{G93A}-expressing astrocyte in the presence of XeC. Note that the treatment with XeC abolished the $[Ca^{2+}]_i$ response induced by both TAT-BH4 and DHPG in the majority of cells analyzed ($98.5 \pm 1.5\%$; $n = 53$ cells analyzed; $n = 8$ experiments). (**D**) Summary (mean $\pm$ s.e.m.) of >50 cells in multiple trials representing the average oscillation frequency induced by DHPG (100 μM) or TAT-BH4 (0.5 μM) plus DHPG per each genotype and treatment.

4.0% of oscillatory responding cells, $n = 53$ cells analyzed; $n = 8$ experiments; Fig. 4C), thus indicating that TAT-BH4 controls the $[Ca^{2+}]_i$ signaling by modulating the IP$_3$R activity.

Administration of the group I mGluR agonist DHPG (100 μM), 30 min after the application of TAT-BH4, triggered the typical single $[Ca^{2+}]_i$ transient in 99% of the cells, followed by persistent $[Ca^{2+}]_i$ oscillations (Fig. 4A and B). The average oscillation frequency was similar to that of wild-type cells (Fig. 4A and D), and these effects were fully dependent on the release of Ca^{2+} from the internal stores, as determined by pharmacological experiments (Fig. 4B and C). On the basis of these observations, we conclude that the BH4 domain of Bcl-X$_L$ is sufficient to abolish DHPG-dependent unregulated $[Ca^{2+}]_i$ rises and to restore normal spontaneous and evoked $[Ca^{2+}]_i$ oscillations in ALS astrocytes.

TAT-BH4 protects astrocytes from IP$_3$R-driven toxicity by fine-tuning $[Ca^{2+}]_i$ signaling

In the next set of experiments, we evaluated whether the restoration of physiological $[Ca^{2+}]_i$ oscillations in hSOD1^{G93A}-expressing astrocytes correlated with a glioprotective effect of TAT-BH4 against mGluR5-dependent excitotoxic damage. Spinal astrocytic cultures from hSOD1^{G93A} or wild-type mice were pre-incubated in the absence or presence of 0.5 μM TAT-BH4 for 30 min. The peptide in excess was then removed and cells were exposed to 100 μM DHPG or control solution (30 min). In the absence of TAT-BH4, we confirmed that DHPG induces the release of cytochrome *c* from mitochondria (Fig. 5A), an event that is associated to caspase-3 activation and nuclear condensation selectively in
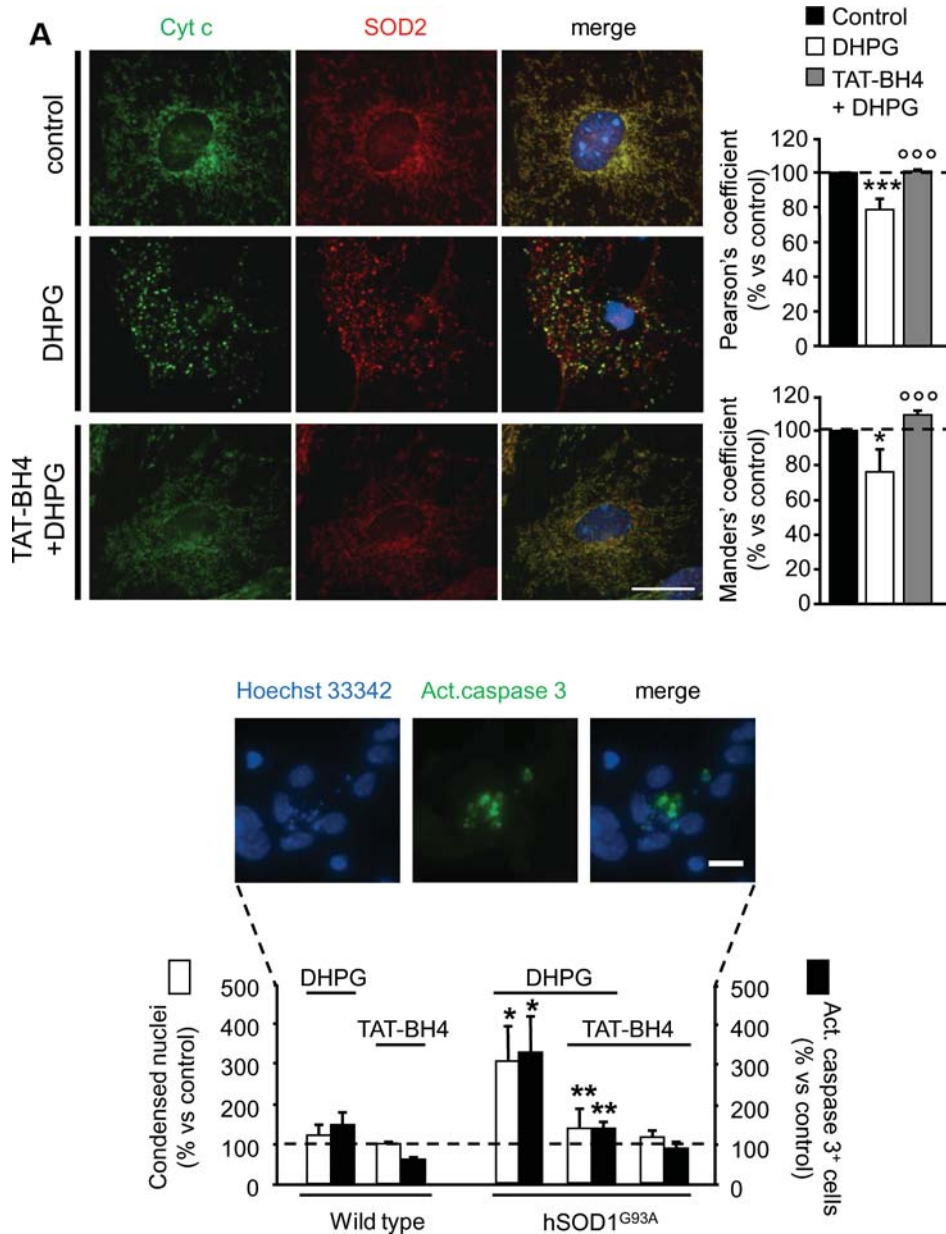
Figure 5. Glioprotective effect of the TAT-BH4 peptide against DHPG toxicity. (**A**, **B**) Astrocyte cultures from wild-type or hSOD1^{G93A} mice were pre-treated in the absence or presence of 0.5 μM TAT-BH4 for 30 min and then incubated with 100 μM DHPG. (A) Representative images of hSOD1^{G93A}-expressing astrocytes double-immunolabeled for cytochrome *c* (Cyt *c*, green) and the mitochondrial marker manganese superoxide dismutase (SOD2, red); nuclei were stained with Hoechst 33342 (blue). Scale bar, 20 μm. Note that the treatment with DHPG causes mitochondrial disarrangement and release of Cyt *c*, as revealed by the loss of co-localization between Cyt *c* and SOD2 immunosignals. Pre-treatment with TAT-BH4 restores the complete co-localization of the two proteins, similar to the situation in control conditions. Histograms show the mean Pearson's and Manders' coefficients as calculated using JACoP plug-in of ImageJ software in the different experimental conditions (see Materials and Methods) (78). Data (mean ± s.e.m.) are expressed as percentage of Pearson's and Manders' coefficients of control condition (control values: Pearson's coefficient: 0.864 ± 0.008; Manders' coefficient (M2): 0.728 ± 0.016, $n = 25$ cells for each experimental condition) (*$P < 0.05$ and ***$P < 0.0001$ versus control, °°°$P < 0.0001$ versus DHPG, one-way ANOVA followed by Bonferroni *post-hoc* test). (B) Treatment with DHPG induces an increment in the percentage of hSOD1^{G93A}-expressing astrocytes with nuclear condensation and caspase-3 activation as compared with wild-type cells. Data (mean ± s.e.m.) are expressed as % of control, i.e. the corresponding culture type challenged with saline (control values: cells with condensed nuclei: wild-type: 0.96 ± 0.07%; hSOD1^{G93A}: 0.98 ± 0.13%; cells immunopositive for active caspase-3: wild-type: 0.32 ± 0.08%; hSOD1^{G93A}: 0.33 ± 0.07%, $n = 3$ in triplicate). The presence of TAT-BH4 significantly reduced the percentage of ALS astrocytes showing nuclear condensation and caspase-3 activation (*$P < 0.05$ versus control; **$P < 0.05$ versus DHPG, one-way ANOVA followed by Bonferroni *post-hoc* test). Above the histograms, representative images of astrocytes with condensed nuclei (Hoechst 33342) and immunopositive for the active caspase-3. Scale bar, 20 μm.

mutant SOD1-expressing astrocytes (Fig. 5B) (25). However, when astrocytes deriving from hSOD1^{G93A} mice were pre-treated with the TAT-BH4 peptide, we detected a significant reduction in both the release of cytochrome *c* and the apoptotic parameters (Fig. 5A and B). To ascertain whether the identified alterations in intracellular Ca^{2+} signaling strictly
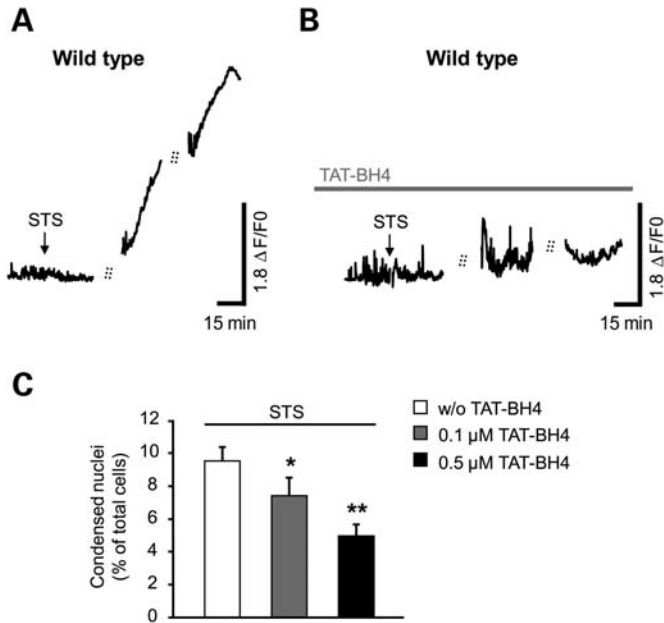
Figure 6. The TAT-BH4 peptide restores normal $[Ca^{2+}]_i$ signaling and survival in STS-treated wild-type astrocytes in culture. (**A**) Typical single-cell $[Ca^{2+}]_i$ response of wild-type astrocytes to application of 1 μM STS. Note that the majority of cells ($n = 81$ cells analyzed; $n = 5$ experiments) responded with an abnormal long-lasting calcium rise that reaches the plateau in about 75–80 min ($\Delta F/F_0$: 3.52 ± 0.22). (**B**) Representative single-cell $[Ca^{2+}]_i$ transients obtained in wild-type astrocytes treated with TAT-BH4 peptide (0.5 μM) for 30 min before the local application of STS (1 μM; black trace). Note that TAT-BH4 reduced the persistent $[Ca^{2+}]_i$ rise evoked by STS (−72%; $n = 76$ cells analyzed; $n = 5$ experiments) and restored $[Ca^{2+}]_i$ oscillations. (**C**) Astrocyte cultures were pre-incubated for 30 min in the absence (w/o TAT-BH4) or in the presence of increasing concentrations of TAT-BH4 (0.1 or 0.5 μM) and then treated with STS (1 μM) for 6 h. The latter caused an increment in the percentage of cells with nuclear condensation, whereas the peptide reduced the number of apoptotic cells in a dose-dependent manner. Data (mean ± s.e.m.) are expressed as % of total cells ($n = 3$ in duplicate) ($^*P < 0.05$ and $^{**}P < 0.01$ versus STS w/o TAT-BH4, one-way ANOVA followed by Bonferroni *post-hoc* test).

correlated with the mGluR5-dependent gliodegenerative process, we subsequently performed single-cell $[Ca^{2+}]_i$ imaging of wild-type astrocytes stimulated with staurosporine (STS), a well-established pro-apoptotic stimulus that leads to cell death by causing IP_3R-dependent Ca^{2+} leak from the intracellular stores via the activation of IP_3Rs (38,58–61). Similar to DHPG-stimulated ALS astrocytes, we found that STS (1 μM) triggers a persistent increase in cytosolic calcium that reaches the plateau in about 75–80 min. This event is coupled to the absence of evident calcium oscillations (Fig. 6A). However, when STS was administered 30 min after the application of TAT-BH4, a significant reduction in the levels of intracellular calcium (−72% with respect to cells treated with STS alone), coupled to the re-establishment of $[Ca^{2+}]_i$ oscillations, was observed (Fig. 6B). Interestingly, the variations in $[Ca^{2+}]_i$ occurring in the absence or presence of TAT-BH4 quantitatively correlated with astrocyte degeneration. Indeed, in parallel experiments, we found that treating astrocytes with STS (1 μM) in the absence of the peptide caused cell death, as determined by nuclear condensation (Fig. 6C). When cells were pre-incubated with increasing

concentrations of TAT-BH4 (0.1 and 0.5 μM, 30 min), however, astrocyte degeneration was potently inhibited in a dose-dependent fashion (Fig. 6C). In view of the impact of STS on IP3Rs, we conclude that astroglial transduction of TAT-BH4 is effective in protecting the cells against IP_3-R-driven cell death.

In vivo administration of TAT-BH4 reduces astrocyte degeneration, slightly postpones disease onset and improves both motor performance and survival of hSOD1[G93A] mice

On the basis of the above observations, we next decided to assess the therapeutic potential of TAT-BH4 *in vivo* on ALS transgenic mice. Starting at the age of 40 days, hSOD1[G93A] animals were treated daily with TAT-BH4 (5 mg/kg intraperitoneally) or equivalent volumes of vehicle solution (saline). Thereafter, mice were monitored daily for survival and twice a week for both decline in body weight and motor performance, using the rotarod test. As weight gain stops at the time of disease onset, the peak in the body weight curve was taken as the earliest measure of the onset of the disease (8,9). According to this criterion, we found that the disease manifestation was slightly, but significantly, delayed in mice injected with TAT-BH4 compared with controls (saline: 99.1 ± 2.9 days; TAT-BH4: 107.5 ± 1.8 days, $n = 14$ per experimental group; $P < 0.05$, Logrank test; Fig. 7A). In addition, animals treated with the peptide performed significantly better in the rotarod tasks throughout life (Fig. 7B) and had a prolonged survival time compared with vehicle-injected mice (saline: 123 ± 2.1 days; TAT-BH4: 138 ± 2.1 days, $n = 14$ per experimental group; $P < 0.001$, Logrank test; Fig. 7C). Immunohistochemical analyses were then performed on spinal cords from a cohort of mice sacrificed at about 100 days of age, i.e. the time of disease onset. Transduction of the peptide was first evaluated at the cellular levels by double immunostaining using antibodies for TAT and the astrocyte- and neuron-specific markers GFAP and microtubule-associated proteins (MAPs), respectively. Although robust immunoreactivity was detected in most astrocytes, motor neurons showed rather heterogeneous staining, with some cells displaying a faint immunosignal (Supplementary Material, Fig. S4C). The expression of mGluR5 was then analyzed on spinal cord sections from both control and peptide-treated hSOD1[G93A] mice double stained for the receptor and GFAP or the neuronal non-phosphorylated neurofilament marker (SMI32). Quantification of mGluR5 immunofluorescence in astrocytes and motor neurons revealed that the expression and distribution of the receptor was unchanged upon treatment with TAT-BH4 in both cell types (mGluR5 expression levels in astrocytes or motor neurons from control hSOD1[G93A] mice was set as 100%; mGluR5 expression levels in TAT-BH4-injected hSOD1[G93A] mouse spinal cords: astrocytes: 97.4 ± 3.1% versus saline, $P = 0.50$, unpaired *t*-test; motor neurons: 96.5 ± 2.4% versus saline, $P = 0.47$, unpaired *t*-test, $n = 6$ cells from three mice). To determine whether the positive effect of the peptide on disease onset and progression was related to the identified degenerative process of astrocytes, we next investigated the impact of TAT-BH4 on both glial and neuronal cells.
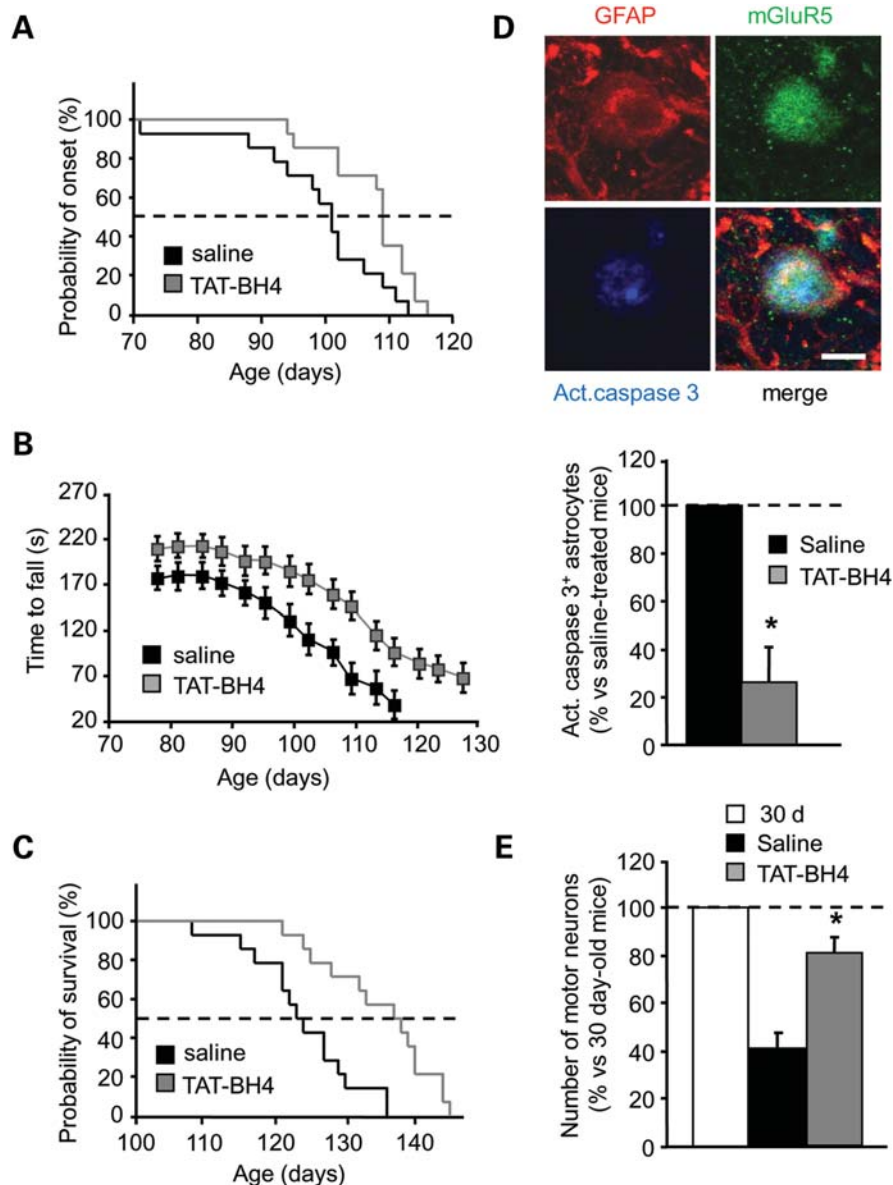
Figure 7. Treatment of hSOD1^{G93A} mice with the TAT-BH4 peptide alleviates the manifestations of the disease. (**A**) Kaplan–Meier curves represent the ages at which the disease onset (peak body weight) was reached for saline-treated and TAT-BH4-treated (TAT-BH4, 5 mg/kg i.p. daily) hSOD1^{G93A} mice ($n = 14$ mice for each condition). Note that the onset of symptoms in TAT-BH4-treated mice is significantly retarded by 8 days compared with controls ($P < 0.05$, Logrank test). (**B**) Rotarod performance of transgenic hSOD1^{G93A} mice treated with saline or TAT-BH4 ($n = 14$ mice for each condition). Motor performance is significantly improved in hSOD1^{G93A} mice treated with the peptide compared with controls. Data (mean $\pm$ s.e.m.) are expressed as the average time of permanence on the rod of all animals ($P < 0.05$, repeated-measures ANOVA). (**C**) Survival analysis of saline- and TAT-BH4-treated hSOD1^{G93A} mice ($n = 14$ mice for each condition). The lifespan is significantly extended by 15 days ($P < 0.001$, Logrank test). The dotted lines in A and C indicate the median values in the two mouse populations. (**D**) Representative images of a degenerating astrocyte as defined by GFAP (red) and showing active caspase-3 (blue) and mGluR5 (green) immunoreactivity. Scale bar, 10 μm. Histograms indicate the percentage of spheroid astrocytes that are positive for the active caspase-3 in sections from 100-day-old saline-treated or TAT-BH4-treated hSOD1^{G93A} mice ($n = 3$ mice for each condition). Data (mean $\pm$ s.e.m.) are expressed as % of total active caspase-3-positive spheroid astrocytes present in 100-day-old saline-treated hSOD1^{G93A} mice (46 ± 16 active-caspase-3-positive astrocytes). The number of caspase-3-positive cells is significantly lower in the TAT-BH4-treated group (*$P < 0.05$ versus saline, unpaired *t*-test). (**E**) Histograms show the number of motor neurons in spinal cord sections from 30-day-old or 100-day-old saline-treated or TAT-BH4-treated hSOD1^{G93A} mice ($n = 3$ mice for each condition). Data (mean $\pm$ s.e.m.) are expressed as % of total motor neurons present in 30-day-old hSOD1^{G93A} mice (596.1 ± 96.14; *$P < 0.05$ versus saline, one-way ANOVA followed by Bonferroni *post-hoc* test).

We found that the treatment with the peptide significantly reduced the number of spheroid astrocytes immunopositive for the active caspase-3 located in the motor neuron microenvironment (-74% with respect to saline-treated mice, Fig. 7D), but not the overall number of GFAP-positive astrocytes distributed throughout the spinal ventral horns (saline: 987.7 ± 29.1 cells/mm^2; TAT-BH4: 917.9 ± 33.1 cells/mm^2; $n = 18$ fields from three mice; $P = 0.07$, unpaired *t*-test).

Noteworthy, the quantity of CD11b-immunopositive microglial cells were slightly, but significantly, decreased upon chronic injection of TAT-BH4 (saline: 1194 ± 20 cells/mm^2; TAT-BH4: 1040.7 ± 20.4 cells/mm^2; $n = 18$ fields from three mice; $P < 0.05$, unpaired t-test). This result correlated with the preservation of a greater number of motor neurons (Fig. 7E). On the basis of these findings, we conclude that the treatment with TAT-BH4 slightly delays the onset of the disease, slows the rate of disease progression and reduces degeneration of astrocytes and motor neurons.

DISCUSSION

Considerable evidence indicates that degeneration of motor neurons in ALS is non-cell-autonomous and requires combined alterations in motor neurons and the surrounding non-neuronal cells, particularly astrocytes (6–11,13–23). In this context, we and others previously described a degenerative process of the astrocytes located in the neighborhood of motor neurons in the spinal cord of hSOD1^{G93A} transgenic mice (24,25). We postulated that astroglial loss may deprive the adjacent motor neurons of the optimal microenvironment and, thus, exacerbate their degeneration.

In this study, we further expanded this observation by analyzing post-mortem tissues from sporadic ALS patients. We found that gliodegeneration is not only a peculiarity of the hSOD1^{G93A} mouse model of familial ALS, but occurs also in the sporadic form of the disease, thus corroborating the relevance of this phenomenon in the context of the human pathology. Astrocyte death is not an unusual event in neurodegenerative disorders characterized by a neuroinflammatory response and may represent a self-protective mechanism to limit the intensity and duration of reactive gliosis (62,63). However, loss of specific subpopulations of astroglia or those cells located in strategic positions may compromise neuronal activity and survival by restraining their neurosupportive factors and functions (64).

On a mechanistic standpoint, prior studies *in vitro* implied the involvement of mGluR5 in the process of astroglial damage (25). In keeping with this, here we found that dying astrocytes are strongly immunoreactive for mGluR5 in the spinal cord of both symptomatic hSOD1^{G93A} mice and autoptic sALS cases, suggesting that this receptor may be involved in the gliodegenerative process also *in vivo*.

The stage at which mGluR5 becomes relevant for ALS progression was then investigated by determining the degree of the receptor expression in the spinal cord of hSOD1^{G93A} ALS mice. The overall levels of mGluR5 resulted significantly enhanced in young, pre-symptomatic ALS animals, thus indicating that the receptor is likely to play a major role during the early phases of the disease. Noteworthy, also neonatal astrocytic cultures, prepared from the spinal cord of hSOD1^{G93A} mice, displayed increased expression of mGluR5 transcripts, confirming that the up-regulation of mGluR5 occurs during the early development in ALS astroglia.

In normal astrocytes, the activation of group I mGluRs, including mGluR5, triggers the formation of IP$_3$ and the consequent release of Ca^{2+} from the ER, resulting in intracellular calcium oscillations (49,50).

In general, Ca^{2+} released from the intracellular stores is rapidly taken up by closely juxtaposed mitochondria. An increase in mitochondrial Ca^{2+} then fine tunes the organelle function to the enhanced needs of the activated cells (31,65). However, non-physiological release of Ca^{2+} from the ER, in response to IP$_3$ production, may result in mitochondrial Ca^{2+} overload and, thus, recruit mitochondria to the apoptotic cascade (27–31,38). Consistent with this, here we found that stimulating hSOD1^{G93A}-expressing astrocytes with DHPG, a group I mGluR agonist, does not produce calcium spiking, but causes in about 99% of the cells a persistent [Ca^{2+}]$_i$ rise, which is exceptionally elevated in a number of cells. This event is fully dependent on the Ca^{2+} efflux from the ER, suggesting that not only the expression of mGluR5 is altered in mutant SOD1 astrocytes, but also the function of its downstream signaling effectors. Misfolded mutant SOD1s were recently reported not to cause Ca^{2+} handling defects in spinal cord mitochondria (24,25,66,67). However, we postulated that an increased release of ER Ca^{2+} in ALS astrocytes may enhance mitochondrial Ca^{2+} uptake and, thus, trigger astroglial cell death. In keeping with this, here we found that the abnormal rise in cytosolic calcium triggered by DHPG correlates with mitochondrial disarrangement, release of cytochrome *c* and degeneration of a fraction of ALS astrocytes. These results are fully consistent with a previous study describing reduced capacity of mitochondria from the spinal cord of mutant SOD1 mice to survive repetitive Ca^{2+} challenge (68). Furthermore, they are in agreement with a recent report describing mitochondrial dysfunction in mutant SOD1-expressing astrocytes (19).

The IP$_3$R/Ca^{2+}/apoptosis connection was then further investigated by stimulating wild-type astrocytes with STS, another apoptotic stimulus that triggers cell death by disrupting the IP$_3$ receptor-mediated calcium homeostasis (58–61,69). Here we found that the treatment with STS causes a sustained increase in [Ca^{2+}]$_i$, which is similar to that triggered by DHPG in ALS astrocytes, but to higher levels. Also in this case, the [Ca^{2+}]$_i$ rise is associated to degeneration of a significant number of cells. Interestingly, the [Ca^{2+}]$_i$ released by hSOD1^{G93A}-expressing or wild-type astrocytes treated with DHPG or STS, respectively, quantitatively correlated with the extent of cell death. Thus, we infer that, in both conditions, it is the persistent IP$_3$R-mediated Ca^{2+} release from the intracellular stores that underlies astrocyte degeneration. This finding is particularly interesting in view of previous observations indicating that IP$_3$R2, the isoform predominantly (or selectively) expressed in astrocytes (70), is up-regulated in cells from sporadic ALS patients (71).

Fine tuning of the intracellular Ca^{2+} homeostasis by the anti-apoptotic Bcl-2/Bcl-X$_L$ proteins was described to control cell death mechanisms (29,31,38). Although the BH4 domain of Bcl-2 was reported to be necessary and sufficient to prevent apoptosis by regulating the efflux of calcium from the ER (35), the role of the N-terminal BH4 domain of Bcl-X$_L$ in modulating pro-survival Ca^{2+} signals was not explored. In this study, we thus investigated the impact of the BH4 domain of Bcl-X$_L$ on astrocyte Ca^{2+} signaling by exploiting a biologically active BH4 peptide fused to the HIV-1 TAT protein. Consistent with previous evidence using the full-length Bcl-X$_L$ protein (36,37), we found that

TAT-BH4 modulates the IP_3R-dependent Ca^{2+} release from the ER and restores spontaneous Ca^{2+} oscillations in mutant SOD1-expressing astrocytes. This tight control of IP_3Rs by the peptide prevents the DHPG-induced aberrant release of Ca^{2+} from the intracellular stores and protects the cells from excitotoxic damage.

The fact that TAT-BH4 re-establishes Ca^{2+} oscillations and inhibits astrocyte degeneration in a dose-dependent manner also upon STS treatment confirms the efficacy of the peptide towards IP_3R-dependent astroglial cell death, thus establishing a correlation between the deranged mGluR5 Ca^{2+} signaling and the degenerative process of hSOD1[G93A]-expressing astrocytes. Further studies are clearly necessary to clarify the mechanisms by which hSOD1[G93A] directly or indirectly interferes with mGluR5 signaling in astroglial cells. However, on the basis of our results, we can hypothesize that the reduction in Bcl-X_L expression identified in ALS astrocytes may account, at least in part, for the loss of intracellular Ca^{2+} homeostasis identified in the mutant cells. Furthermore, additional and complementary hypotheses can be formulated from the available evidence. For example, a recent study indicates that conformational changes of Bcl-2 and exposure of the pro-apoptotic BH3 domain occur at the mitochondrial membrane in mutant SOD1-expressing cells (72). Considering that the BH3-containing pro-apoptotic members of the Bcl-2 family proteins were implied in the regulation of ER Ca^{2+} signaling (73), one can postulate that the occurrence of a similar event at the ER, due to the accumulation of misfolded mutant SOD1s within astrocytes (24,25,66,67), might cause derangement of the intracellular Ca^{2+} homeostasis and trigger Ca^{2+}-dependent cell death. In both cases, re-introduction of Bcl-X_L BH4, in the form of cell-permeable peptide, overcomes the biochemical and functional defects triggered by mutant SOD1 in astrocytes either by reinforcing the endogenous Bcl-X_L or by counteracting the deleterious effects of the BH3 domain.

A crucial indication that astrocyte alterations are implicated in ALS progression *in vivo* came from the original observation that reducing mutant SOD1 expression within astrocytes significantly affects the late disease progression in hSOD1[G37R] transgenic mice (9). More recent evidence, using the same genetic approach, then suggested that ablation of the mutant protein specifically in astrocytes affects disease onset and early disease progression in hSOD1[G85R] animals (10). Although both studies highlight the importance of astroglial cells in familial ALS, they also suggest that distinct mutations may differently influence the course of the disease. A role for hSOD1[G93A] astrocytes in triggering motor neuron degeneration and ALS symptoms *in vivo* has been clearly demonstrated in a recent study using a cell transplantation strategy (11). However, no information is currently available on the impact of hSOD1[G93A] astroglial cells on disease progression.

Since intraperitoneal injection of TAT-conjugated proteins was previously reported to allow an efficient transduction of the fusion proteins into the brain cells (56), here we investigated the impact on both gliodegeneration and disease progression of the TAT-BH4 peptide in hSOD1[G93A] mice, using this route of administration. The dosage of 5 mg/kg of body weight was selected in our preclinical trial for two reasons. First, the acute treatment of mice with equivalent doses of TAT-Bcl-X_L resulted protective against other neurodegenerative conditions, such as ischemic injury of the brain (74). Second, the chronic administration of similar doses of TAT-conjugated proteins, on a daily basis, was reported to produce no signs of neurological impairment or systemic distress in wild-type mice, thus suggesting no obvious toxicity of the TAT protein (56). In hSOD1[G93A] mice, we found that the prolonged treatment with the peptide, starting at the pre-symptomatic stage of the disease, slightly delays the onset of the disease and improves both motor performance and survival of ALS transgenic mice. These effects are not accompanied by a reduction in the expression of mGluR5 in the different cell types, possibly because the peptide acts on its downstream effectors. However, they correlate with a reduction in the number of astrocytes located in proximity of motor neurons and expressing the apoptotic effector caspase-3. Noteworthy, the overall number of astroglial cells that are placed in more distant positions compared with motor neuronal somas were unaffected by the treatment. In contrast, microglial cells were moderately, but significantly, reduced, probably as a consequence of diminished astrocyte degeneration. These results correlate with the preservation of a greater number of motor neurons. Whether the effect towards motor neurons is a consequence of the maintenance of a larger number of neuro-supportive astrocytes in the motor neuron microenvironment or can be partially ascribed to a direct action of the peptide on these cells remains to be elucidated. Nevertheless, comparative analyses of internalized TAT-BH4 *in situ* indicate that the peptide is more easily captured by astrocytes than motor neurons, suggesting that the major effect may be at the astroglial level.

In conclusion, our results indicate for the first time the BH4 domain of Bcl-X_L as a novel therapeutic for ALS. Furthermore, this study points at cell-permeable peptides as an innovative class of drugs suitable for mechanistic studies and endowed with a potential for curing ALS.

MATERIALS AND METHODS

Transgenic mice and breeding

Transgenic mice expressing human SOD1[G93A] (B6SJL-TgN(SOD1-G93A)1Gur) were purchased from the Jackson Laboratories. The colonies were maintained by breeding hemizygote males to wild-type C57Bl6/SJL F1 hybrid females. Offspring were genotyped and used for subsequent studies. Animal procedures were approved by the Italian Ministry of Health.

ALS biopsy material

Autoptic tissues from sALS cases were obtained from the Department of Pathology of the Academic Medical Center (University of Amsterdam) and the Netherlands ALS Tissue Bank. Informed consent was obtained for the use of brain tissue. Tissue was acquired and used in a manner compliant with the Declaration of Helsinki. All autopsies took place within 12 h after death.

All cases were reviewed independently by two neuropathologists, and the diagnosis of ALS was confirmed according to the previously described histopathological criteria (75).

Tissue preparation and immunohistological analysis

For mouse tissue preparation, the spine was taken and immersed in 4% buffered paraformaldehyde for 24 h; spinal cord was extracted, the lumbar tract was removed and either paraffin embedded or cryoprotected in 30% sucrose before freezing. For human tissue preparation, spinal cord was removed and 0.5-cm thick slices were taken from the cervical (C7), thoracic (T4 and T8) and lumbar (L1) levels. Slices were fixed in 10% buffered formalin and embedded in paraffin. Mouse or human spinal cords were sectioned at $5-10 \, \mu m$ and used to perform different immunostaining. On selected sections, the following primary antibodies were used: GFAP (mouse monoclonal antibody, 1:50, Dako), SMI32 (mouse monoclonal antibody, 1:500, Covance), MAPs (rabbit polyclonal antibody, 1:200, Sigma), CD11b (rat monoclonal antibody, 1:500, Serotec), mGluR5 (rabbit polyclonal antibody, 1:100, MBL International Corporation); active caspase-3 (rabbit polyclonal antibody, 1:50, Cell Signalling Technology), TAT (mouse monoclonal antibody, 1:10, kindly provided by Prof. Dag Helland, University of Bergen, Norway). For active caspase-3 immunostaining, a Tyramide Amplification System Kit was used (Perkin Elmer, Inc.). To resolve background problems with mouse primary antibody on murine tissues, a Vector® M.O.M.™ Immunodetection Kit (Vector) was used. For histopathological analysis, serial sections were either immunostained for GFAP/active caspase-3 or treated with 0.5% cresyl violet (Sigma-Aldrich) to detect motor neuron Nissl substance. GFAP/active caspase-3-positive astrocytes and motor neurons were counted for a total of nine disectors using an unbiased stereologic physical disector technique (76).

Z-axis image stacks (*z*-step size: $0.5 \, \mu m$) were collected to generate three-dimensional data sets of spinal cord sections on an MRC 1024 Bio-Rad confocal microscope with a $63 \times$ Plan Neofluar NA1,25 oil-immersion objective in condition of optimal iris diameter as defined by LaserSharp 2000 software.

Quantitative analysis of punctuate mGluR5, GFAP or CD11b staining was performed on confocal acquired images (1024×1024 pixels) of the spinal cord ventral horns from both wild-type and hSOD1[G93A] animals using ImageJ software (National Institutes of Health, Bethesda, MD, http://rsb.info.nih.gov/ij/). After establishing an intensity threshold, the software calculated the percentage of area occupied by mGluR5, GFAP or CD11b staining by dividing the area of immunopositivity by the total area. To quantify the number of GFAP and CD11b immunopositive cells in the ventral horns of the lumbar spinal cord, 18 fields/mouse from three animals per each experimental condition were analyzed by ImageJ software (10).

Astrocyte cultures

Primary astrocyte cultures (>99% GFAP-positive) were prepared from the spinal cord of newborn mice (hSOD1[G93A] or wild-type littermates) as previously described (25). Once the cultures reached the confluence, they were re-plated at the optimal density either in 24-well plates or 35-mm Petri dishes containing glass coverslips and maintained in Minimal Essential Medium (MEM, Gibco) supplemented with 10% fetal bovine serum (Sigma-Aldrich).

Quantitative RT–PCR

Total RNA was extracted from animal tissues or confluent astrocytes in culture using RNeasy Mini Kit (Qiagen) according to the manufacturer's guidelines. One microgram of tissue- or astrocyte-extracted total RNA was reverse-transcribed using iScript cDNA Synthesis Kit according to the manufacturer's instructions (Bio-Rad). Two nanograms of the resulting cDNAs were analyzed by quantitative PCR using the SsoFast EvaGreen Supermix on a CFX96 Real-Time PCR Detection System (BIO-RAD). mGluR5-encoding transcripts were detected using primers 5′-mGluR5-Car (5′-AGCTGTTTT GTCCACATAT) and 3′-mGluR5-Car (5′-CCAGAGAGTG TTGAGTTAG). The housekeeping gene hypoxanthine guanine phosphoribosyl transferase (HPRT) was chosen as a reference and its mRNA was detected using primers 5′-HPRT (5′-TGAATCACGTTTGTGTCATTA) and 3′-HPRT (5′-TTC AACTTGCGCTCATCTTAG).

$[Ca^{2+}]_i$ imaging

Astrocytes were plated (2.5×10^4 cells/35 mm Petri dish) on glass coverslips and used $2-3$ days later as already shown (77). Before imaging, cells were loaded with $5 \, \mu M$ Fluo4-AM (Molecular Probes) for $15-20$ min at $37°C$ in a HEPES-KRH buffer containing (in mM): NaCl 116, KCl 4, $MgCl_2$ 1, $CaCl_2$ 1.8, HEPES acid 10, glucose 25 (pH 7.4) and then allowed to de-esterify for 10 min. After several washes, coverslips were mounted in an open perfusion micro-incubator (PDMI-2, Harvard Apparatus) set at $37°C$ on the stage of the optical recording microscope. During experiments, cells were continuously perfused with HEPES-KRH (1 ml/min), and stimuli were applied via a software-controlled micro-perfusion fast-step device (100 μl/min, Warner Instrument Corp.) A Zeiss Axiovert 200 inverted fluorescence microscope was modified to allow EPI illumination (Visitron Systems). Fluo4 fluorescence was recorded through a $63 \times$ or $40 \times$ objectives lens (Zeiss, Neofluar $63 \times$/1.25 Oil, Neofluar $40 \times$/1.3 Oil) and directed through a Zeiss filter set 10 (BP $450-490$; BP $515-565$) at 200 or 400 ms intervals by imaging with excitation light at 488 nm generated by a polychromator illumination system (Visichrome, Visitron Systems). Video images, digitized with MetaFluor, were analyzed with MetaMorph software (Universal Imaging). Temporal dynamics of Fluo4 fluorescence have been expressed as background-subtracted $\Delta F/F_0$ (%), where F_0 represents the fluorescence level of the cells before stimulation and ΔF the change in fluorescence occurring during the stimulus.

Pharmacological treatments *in vitro*

To assess the ability of TAT-BH4 to penetrate into cells, astrocytes (8×10^4 cells/well) were plated in 24-well plates containing glass coverslips. Cultures were treated with 10 μg/ml

Hoechst 33342 (Sigma) for 15 min, quickly washed and incubated with 0.5 μM L-TAT-BH4 (TAT$_{48-57}$ conjugated to the BH4 domain of Bcl-X$_L$) either unconjugated or conjugated with 5(6)-carboxyfluorescein (FAM, Primm srl) for 30 min. Peptides in excess were subsequently removed, cells were washed and immediately fixed (methanol:acetone, 1:1 for 10 min) or maintained in culture for 24 h and then fixed. The presence of the peptides inside the cells was evaluated by a digital camera (DFC 310 FX, Leica Microsystem) mounted on a DM5000 B microscope (Leica Microsystem) and analyzed by Leica Application Suite 3.5.0 software.

To test the protective efficacy of TAT-BH4, astrocytes in culture were pre-exposed to different concentrations of the peptide (0.1 and/or 0.5 μM, 30 min), washed and then treated with DHPG (100 μM, 30 min, Tocris Cookson Ltd) or STS (1 μM, 6 h, Sigma-Aldrich). After removal of DHPG, astrocytes were allowed to recover at 37°C for 24 h.

Immunocytochemistry and quantitative analysis

Confluent astrocytes were fixed either in 4% buffered paraformaldehyde for 15 min at room temperature or in methanol for 10 min at −20°C. Cells were then immunostained using the following primary antibodies: Bcl-X$_L$ (rabbit polyclonal antibody, 1:50, Santa Cruz), TAT (mouse monoclonal antibody, 1:10, kindly provided by Prof. Dag Helland, University of Bergen, Norway), cytochrome *c* (mouse monoclonal antibody, 1:100, BD Pharmingen), SOD2 (rabbit polyclonal antibody, 1:50, Stressgen), active caspase-3 (rabbit polyclonal antibody, 1:50, Cell Signaling). For quantitative analysis of punctuate Bcl-X$_L$ staining, the total fluorescence of 15 ROI/cell (ROI: 2.09 μm × 2.09 μm) was calculated using ImageJ software ($n = 50$ cells per each experimental condition). Cytochrome *c* release from mitochondria was determined by its co-localization with the mitochondrial protein SOD2 using JACoP plug-in ImageJ. An estimate of the degree of co-localization was obtained by calculating the Pearson's and Manders' coefficients (78).

The toxic effect of DHPG or STS on cultured astrocytes was determined by double staining with the fluorescent nuclear dye Hoechst 33342 and anti-active caspase-3 immunostaining. The number of astrocytes showing condensed nuclei and activated caspase-3, 24 h after the pharmacological challenge, was counted by two independent operators in a blind manner. The number of dying astrocytes was counted in 8–10 microscopic fields (40×) per coverslip and expressed as percentage of the total number of cells present in the field.

Pharmacological treatment *in vivo*

hSOD1^{G93A} mice were administrated daily 5 mg/kg L-TAT-BH4 peptide (GenScript) or vehicle (PBS containing 10% glycerol) intraperitoneally starting at the age of 40 days ($n = 14$ mice for each condition). Mice were thereafter kept under daily observation and weighted twice a week. Age of disease onset was retrospectively determined as the time when mice reached the peak in the body weight. Motor performance was assessed twice a week by rotarod test starting at the age of 50 days. Briefly, animals were placed on an accelerating rod (Ugo Basile) and the time each mouse remained on the rod was recorded. The average of three independent trials per session was used for further analysis of the data. End stage was defined as the time in which animals were unable to right themselves within 30 s when placed on their side.

Statistics. Data are represented as mean ± s.e.m. and statistical significance was verified using GraphPad Prism® software. Paired or unpaired 2-tailed *t*-test was used for comparisons between two groups; one-way or two-way analysis of variance (ANOVA) followed by Bonferroni *post-hoc* test was used for comparisons of multiple groups; repeated-measures two-way ANOVA was used for behavioral test; the Logrank test was used for disease onset and survival analysis.

SUPPLEMENTARY MATERIAL

Supplementary Material is available at *HMG* online.

REFERENCES

1. Attwell, D., Buchan, A.M., Charpak, S., Lauritzen, M., Macvicar, B.A. and Newman, E.A. (2010) Glial and neuronal control of brain blood flow. *Nature*, **468**, 232–243.
2. Eroglu, C. and Barres, B.A. (2010) Regulation of synaptic connectivity by glia. *Nature*, **468**, 223–231.
3. Verkhratsky, A., Orkand, R.K. and Kettenmann, H. (1998) Glial calcium: homeostasis and signaling function. *Physiol. Rev.*, **78**, 99–141.
4. Perea, G., Navarrete, M. and Araque, A. (2009) Tripartite synapses: astrocytes process and control synaptic information. *Trends Neurosci.*, **32**, 421–431.
5. Halassa, M.M. and Haydon, P.G. (2010) Integrated brain circuits: astrocytic networks modulate neuronal activity and behavior. *Annu. Rev. Physiol.*, **72**, 335–355.
6. Clement, A.M., Nguyen, M.D., Roberts, E.A., Garcia, M.L., Boillee, S., Rule, M., McMahon, A.P., Doucette, W., Siwek, D., Ferrante, R.J. *et al.* (2003) Wild-type nonneuronal cells extend survival of SOD1 mutant motor neurons in ALS mice. *Science*, **302**, 113–117.
7. Beers, D.R., Henkel, J.S., Xiao, Q., Zhao, W., Wang, J., Yen, A.A., Siklos, L., McKercher, S.R. and Appel, S.H. (2006) Wild-type microglia extend survival in PU.1 knockout mice with familial amyotrophic lateral sclerosis. *Proc. Natl Acad. Sci. USA*, **103**, 16021–16026.
8. Boillee, S., Yamanaka, K., Lobsiger, C.S., Copeland, N.G., Jenkins, N.A., Kassiotis, G., Kollias, G. and Cleveland, D.W. (2006) Onset and progression in inherited ALS determined by motor neurons and microglia. *Science*, **312**, 1389–1392.
9. Yamanaka, K., Chun, S.J., Boillee, S., Fujimori-Tonou, N., Yamashita, H., Gutmann, D.H., Takahashi, R., Misawa, H. and Cleveland, D.W.

(2008) Astrocytes as determinants of disease progression in inherited amyotrophic lateral sclerosis. *Nat. Neurosci.*, **11**, 251–253.

10. Wang, L., Gutmann, D.H. and Roos, R.P. (2011) Astrocyte loss of mutant SOD1 delays ALS disease onset and progression in G85R transgenic mice. *Hum. Mol. Genet.*, **20**, 286–293.

11. Papadeas, S.T., Kraig, S.E., O'Banion, C., Lepore, A.C. and Maragakis, N.J. (2011) Astrocytes carrying the superoxide dismutase 1 (SOD1G93A) mutation induce wild-type motor neuron degeneration *in vivo*. *Proc. Natl Acad. Sci. USA*, **108**, 17803–17808.

12. Ilieva, H., Polymenidou, M. and Cleveland, D.W. (2009) Non-cell autonomous toxicity in neurodegenerative disorders: ALS and beyond. *J. Cell Biol.*, **187**, 761–772.

13. Rothstein, J.D., Martin, L.J. and Kuncl, R.W. (1992) Decreased glutamate transport by the brain and spinal cord in amyotrophic lateral sclerosis. *N. Engl. J. Med.*, **326**, 1464–1468.

14. Van Damme, P., Bogaert, E., Dewil, M., Hersmus, N., Kiraly, D., Scheveneels, W., Bockx, I., Braeken, D., Verpoorten, N., Verhoeven, K. *et al.* (2007) Astrocytes regulate GluR2 expression in motor neurons and their vulnerability to excitotoxicity. *Proc. Natl Acad. Sci. USA*, **104**, 14825–14830.

15. Nagai, M., Re, D.B., Nagata, T., Chalazonitis, A., Jessell, T.M., Wichterle, H. and Przedborski, S. (2007) Astrocytes expressing ALS-linked mutated SOD1 release factors selectively toxic to motor neurons. *Nat. Neurosci.*, **10**, 615–622.

16. Di Giorgio, F.P., Carrasco, M.A., Siao, M.C., Maniatis, T. and Eggan, K. (2007) Non-cell autonomous effect of glia on motor neurons in an embryonic stem cell-based ALS model. *Nat. Neurosci.*, **10**, 608–614.

17. Di Giorgio, F.P., Boulting, G.L., Bobrowicz, S. and Eggan, K.C. (2008) Human embryonic stem cell-derived motor neurons are sensitive to the toxic effect of glial cells carrying an ALS-causing mutation. *Cell Stem Cell*, **3**, 637–648.

18. Marchetto, M.C., Muotri, A.R., Mu, Y., Smith, A.M., Cezar, G.G. and Gage, F.H. (2008) Non-cell-autonomous effect of human SOD1 G37R astrocytes on motor neurons derived from human embryonic stem cells. *Cell Stem Cell*, **3**, 649–657.

19. Cassina, P., Cassina, A., Pehar, M., Castellanos, R., Gandelman, M., de Leon, A., Robinson, K.M., Mason, R.P., Beckman, J.S., Barbeito, L. *et al.* (2008) Mitochondrial dysfunction in SOD1G93A-bearing astrocytes promotes motor neuron degeneration: prevention by mitochondrial-targeted antioxidants. *J. Neurosci.*, **28**, 4115–4122.

20. Yang, Y., Gozen, O., Watkins, A., Lorenzini, I., Lepore, A., Gao, Y., Vidensky, S., Brennan, J., Poulsen, D., Won Park, J. *et al.* (2009) Presynaptic regulation of astroglial excitatory neurotransmitter transporter GLT1. *Neuron*, **61**, 880–894.

21. Aebischer, J., Cassina, P., Otsmane, B., Moumen, A., Seilhean, D., Meininger, V., Barbeito, L., Pettmann, B. and Raoul, C. (2011) IFNgamma triggers a LIGHT-dependent selective death of motoneurons contributing to the non-cell-autonomous effects of mutant SOD1. *Cell Death Differ.*, **18**, 754–768.

22. Haidet-Phillips, A.M., Hester, M.E., Miranda, C.J., Meyer, K., Braun, L., Frakes, A., Song, S., Likhite, S., Murtha, M.J., Foust, K.D. *et al.* (2011) Astrocytes from familial and sporadic ALS patients are toxic to motor neurons. *Nat. Biotechnol.*, **29**, 824–828.

23. Diaz-Amarilla, P., Olivera-Bravo, S., Trias, E., Cragnolini, A., Martinez-Palma, L., Cassina, P., Beckman, J. and Barbeito, L. (2011) Phenotypically aberrant astrocytes that promote motoneuron damage in a model of inherited amyotrophic lateral sclerosis. *Proc. Natl Acad. Sci. USA*, **108**, 18126–18131.

24. Pasinelli, P., Houseweart, M.K., Brown, R.H. Jr and Cleveland, D.W. (2000) Caspase-1 and -3 are sequentially activated in motor neuron death in Cu,Zn superoxide dismutase-mediated familial amyotrophic lateral sclerosis. *Proc. Natl Acad. Sci. USA*, **97**, 13901–13906.

25. Rossi, D., Brambilla, L., Valori, C.F., Roncoroni, C., Crugnola, A., Yokota, T., Bredesen, D.E. and Volterra, A. (2008) Focal degeneration of astrocytes in amyotrophic lateral sclerosis. *Cell Death Differ.*, **15**, 1691–1700.

26. Rizzuto, R. and Pozzan, T. (2006) Microdomains of intracellular Ca^{2+}: molecular determinants and functional consequences. *Physiol. Rev.*, **86**, 369–408.

27. Hanson, C.J., Bootman, M.D. and Roderick, H.L. (2004) Cell signalling: IP3 receptors channel calcium into cell death. *Curr. Biol.*, **14**, R933–R935.

28. Orrenius, S., Zhivotovsky, B. and Nicotera, P. (2003) Regulation of cell death: the calcium-apoptosis link. *Nat. Rev. Mol. Cell Biol.*, **4**, 552–565.

29. Joseph, S.K. and Hajnoczky, G. (2007) IP3 receptors in cell survival and apoptosis: Ca^{2+} release and beyond. *Apoptosis*, **12**, 951–968.

30. Giacomello, M., Drago, I., Pizzo, P. and Pozzan, T. (2007) Mitochondrial Ca^{2+} as a key regulator of cell life and death. *Cell Death Differ.*, **14**, 1267–1274.

31. Pinton, P., Giorgi, C., Siviero, R., Zecchini, E. and Rizzuto, R. (2008) Calcium and apoptosis: ER-mitochondria Ca^{2+} transfer in the control of apoptosis. *Oncogene*, **27**, 6407–6418.

32. Chen, R., Valencia, I., Zhong, F., McColl, K.S., Roderick, H.L., Bootman, M.D., Berridge, M.J., Conway, S.J., Holmes, A.B., Mignery, G.A. *et al.* (2004) Bcl-2 functionally interacts with inositol 1,4,5-trisphosphate receptors to regulate calcium release from the ER in response to inositol 1,4,5-trisphosphate. *J. Cell Biol.*, **166**, 193–203.

33. Zhong, F., Davis, M.C., McColl, K.S. and Distelhorst, C.W. (2006) Bcl-2 differentially regulates Ca^{2+} signals according to the strength of T cell receptor activation. *J. Cell Biol.*, **172**, 127–137.

34. Rong, Y.P., Aromolaran, A.S., Bultynck, G., Zhong, F., Li, X., McColl, K., Matsuyama, S., Herlitze, S., Roderick, H.L., Bootman, M.D. *et al.* (2008) Targeting Bcl-2-IP3 receptor interaction to reverse Bcl-2's inhibition of apoptotic calcium signals. *Mol. Cell*, **31**, 255–265.

35. Rong, Y.P., Bultynck, G., Aromolaran, A.S., Zhong, F., Parys, J.B., De Smedt, H., Mignery, G.A., Roderick, H.L., Bootman, M.D. and Distelhorst, C.W. (2009) The BH4 domain of Bcl-2 inhibits ER calcium release and apoptosis by binding the regulatory and coupling domain of the IP3 receptor. *Proc. Natl Acad. Sci. USA*, **106**, 14397–14402.

36. Li, C., Wang, X., Vais, H., Thompson, C.B., Foskett, J.K. and White, C. (2007) Apoptosis regulation by Bcl-x(L) modulation of mammalian inositol 1,4,5-trisphosphate receptor channel isoform gating. *Proc. Natl Acad. Sci. USA*, **104**, 12565–12570.

37. White, C., Li, C., Yang, J., Petrenko, N.B., Madesh, M., Thompson, C.B. and Foskett, J.K. (2005) The endoplasmic reticulum gateway to apoptosis by Bcl-X(L) modulation of the InsP3R. *Nat. Cell Biol.*, **7**, 1021–1028.

38. Harr, M.W. and Distelhorst, C.W. (2010) Apoptosis and autophagy: decoding calcium signals that mediate life or death. *Cold Spring Harb. Perspect. Biol.*, **2**, a005579.

39. Hunter, J.J., Bond, B.L. and Parslow, T.G. (1996) Functional dissection of the human Bcl2 protein: sequence requirements for inhibition of apoptosis. *Mol. Cell Biol.*, **16**, 877–883.

40. Lee, L.C., Hunter, J.J., Mujeeb, A., Turck, C. and Parslow, T.G. (1996) Evidence for alpha-helical conformation of an essential N-terminal region in the human Bcl2 protein. *J. Biol. Chem.*, **271**, 23284–23288.

41. Huang, D.C., Adams, J.M. and Cory, S. (1998) The conserved N-terminal BH4 domain of Bcl-2 homologues is essential for inhibition of apoptosis and interaction with CED-4. *EMBO J.*, **17**, 1029–1039.

42. Azzouz, M., Hottinger, A., Paterna, J.C., Zurn, A.D., Aebischer, P. and Bueler, H. (2000) Increased motoneuron survival and improved neuromuscular function in transgenic ALS mice after intraspinal injection of an adeno-associated virus encoding Bcl-2. *Hum. Mol. Genet.*, **9**, 803–811.

43. Guegan, C., Vila, M., Rosoklija, G., Hays, A.P. and Przedborski, S. (2001) Recruitment of the mitochondrial-dependent apoptotic pathway in amyotrophic lateral sclerosis. *J. Neurosci.*, **21**, 6569–6576.

44. Kostic, V., Jackson-Lewis, V., de Bilbao, F., Dubois-Dauphin, M. and Przedborski, S. (1997) Bcl-2: prolonging life in a transgenic mouse model of familial amyotrophic lateral sclerosis. *Science*, **277**, 559–562.

45. Vukosavic, S., Dubois-Dauphin, M., Romero, N. and Przedborski, S. (1999) Bax and Bcl-2 interaction in a transgenic mouse model of familial amyotrophic lateral sclerosis. *J. Neurochem.*, **73**, 2460–2468.

46. Vukosavic, S., Stefanis, L., Jackson-Lewis, V., Guegan, C., Romero, N., Chen, C., Dubois-Dauphin, M. and Przedborski, S. (2000) Delaying caspase activation by Bcl-2: a clue to disease retardation in a transgenic mouse model of amyotrophic lateral sclerosis. *J. Neurosci.*, **20**, 9119–9125.

47. Pasinelli, P., Belford, M.E., Lennon, N., Bacskai, B.J., Hyman, B.T., Trotti, D. and Brown, R.H. Jr (2004) Amyotrophic lateral sclerosis-associated SOD1 mutant proteins bind and aggregate with Bcl-2 in spinal cord mitochondria. *Neuron*, **43**, 19–30.

48. Reyes, N.A., Fisher, J.K., Austgen, K., VandenBerg, S., Huang, E.J. and Oakes, S.A. (2010) Blocking the mitochondrial apoptotic pathway preserves motor neuron viability and function in a mouse model of amyotrophic lateral sclerosis. *J. Clin. Invest.*, **120**, 3673–3679.

49. Gunnarson, E., Song, Y., Kowalewski, J.M., Brismar, H., Brines, M., Cerami, A., Andersson, U., Zelenina, M. and Aperia, A. (2009) Erythropoietin modulation of astrocyte water permeability as a component of neuroprotection. *Proc. Natl Acad. Sci. USA*, **106**, 1602–1607.

50. Zur Nieden, R. and Deitmer, J.W. (2006) The role of metabotropic glutamate receptors for the generation of calcium oscillations in rat hippocampal astrocytes *in situ*. *Cereb. Cortex*, **16**, 676–687.

51. Lytton, J., Westlin, M. and Hanley, M.R. (1991) Thapsigargin inhibits the sarcoplasmic or endoplasmic reticulum Ca-ATPase family of calcium pumps. *J. Biol. Chem.*, **266**, 17067–17071.

52. Plenge-Tellechea, F., Soler, F. and Fernandez-Belda, F. (1997) On the inhibition mechanism of sarcoplasmic or endoplasmic reticulum Ca^{2+}-ATPases by cyclopiazonic acid. *J. Biol. Chem.*, **272**, 2794–2800.

53. Marchaland, J., Cali, C., Voglmaier, S.M., Li, H., Regazzi, R., Edwards, R.H. and Bezzi, P. (2008) Fast subplasma membrane Ca^{2+} transients control exo-endocytosis of synaptic-like microvesicles in astrocytes. *J. Neurosci.*, **28**, 9122–9132.

54. Gafni, J., Munsch, J.A., Lam, T.H., Catlin, M.C., Costa, L.G., Molinski, T.F. and Pessah, I.N. (1997) Xestospongins: potent membrane permeable blockers of the inositol 1,4,5-trisphosphate receptor. *Neuron*, **19**, 723–733.

55. Nakahara, K., Okada, M. and Nakanishi, S. (1997) The metabotropic glutamate receptor mGluR5 induces calcium oscillations in cultured astrocytes via protein kinase C phosphorylation. *J. Neurochem.*, **69**, 1467–1475.

56. Schwarze, S.R., Ho, A., Vocero-Akbani, A. and Dowdy, S.F. (1999) *In vivo* protein transduction: delivery of a biologically active protein into the mouse. *Science*, **285**, 1569–1572.

57. Chang, B.S., Kelekar, A., Harris, M.H., Harlan, J.E., Fesik, S.W. and Thompson, C.B. (1999) The BH3 domain of Bcl-x(S) is required for inhibition of the antiapoptotic function of Bcl-x(L). *Mol. Cell Biol.*, **19**, 6673–6681.

58. Boehning, D., Patterson, R.L., Sedaghat, L., Glebova, N.O., Kuroaki, T. and Snyder, S.H. (2003) Cytochrome *c* binds to inositol (1,4,5) trisphosphate receptors, amplifying calcium-dependent apoptosis. *Nat. Cell Biol.*, **5**, 1051–1061.

59. Assefa, Z., Bultynck, G., Szlufcik, K., Nadif Kasri, N., Vermassen, E., Goris, J., Missiaen, L., Callewaert, G., Parys, J.B. and De Smedt, H. (2004) Caspase-3-induced truncation of type 1 inositol trisphosphate receptor accelerates apoptotic cell death and induces inositol trisphosphate-independent calcium release during apoptosis. *J. Biol. Chem.*, **279**, 43227–43236.

60. Verbert, L., Lee, B., Kocks, S.L., Assefa, Z., Parys, J.B., Missiaen, L., Callewaert, G., Fissore, R.A., De Smedt, H. and Bultynck, G. (2008) Caspase-3-truncated type 1 inositol 1,4,5-trisphosphate receptor enhances intracellular Ca^{2+} leak and disturbs Ca^{2+} signalling. *Biol. Cell*, **100**, 39–49.

61. Zhang, S., Hisatsune, C., Matsu-Ura, T. and Mikoshiba, K. (2009) G-protein-coupled receptor kinase-interacting proteins inhibit apoptosis by inositol 1,4,5-triphosphate receptor-mediated Ca^{2+} signal regulation. *J. Biol. Chem.*, **284**, 29158–29169.

62. Saas, P., Boucraut, J., Quiquerez, A.L., Schnuriger, V., Perrin, G., Desplat-Jego, S., Bernard, D., Walker, P.R. and Dietrich, P.Y. (1999) CD95 (Fas/Apo-1) as a receptor governing astrocyte apoptotic or inflammatory responses: a key role in brain inflammation? *J. Immunol.*, **162**, 2326–2333.

63. Dietrich, P.Y., Walker, P.R. and Saas, P. (2003) Death receptors on reactive astrocytes: a key role in the fine tuning of brain inflammation? *Neurology*, **60**, 548–554.

64. Farina, C., Aloisi, F. and Meinl, E. (2007) Astrocytes are active players in cerebral innate immunity. *Trends Immunol.*, **28**, 138–145.

65. Hajnoczky, G., Robb-Gaspers, L.D., Seitz, M.B. and Thomas, A.P. (1995) Decoding of cytosolic calcium oscillations in the mitochondria. *Cell*, **82**, 415–424.

66. Bruijn, L.I., Becher, M.W., Lee, M.K., Anderson, K.L., Jenkins, N.A., Copeland, N.G., Sisodia, S.S., Rothstein, J.D., Borchelt, D.R., Price, D.L. *et al.* (1997) ALS-linked SOD1 mutant G85R mediates damage to astrocytes and promotes rapidly progressive disease with SOD1-containing inclusions. *Neuron*, **18**, 327–338.

67. Israelson, A., Arbel, N., Da Cruz, S., Ilieva, H., Yamanaka, K., Shoshan-Barmatz, V. and Cleveland, D.W. (2010) Misfolded mutant SOD1 directly inhibits VDAC1 conductance in a mouse model of inherited ALS. *Neuron*, **67**, 575–587.

68. Damiano, M., Starkov, A.A., Petri, S., Kipiani, K., Kiaei, M., Mattiazzi, M., Flint Beal, M. and Manfredi, G. (2006) Neural mitochondrial Ca^{2+} capacity impairment precedes the onset of motor symptoms in G93A Cu/Zn-superoxide dismutase mutant mice. *J. Neurochem.*, **96**, 1349–1361.

69. Kruman, I., Guo, Q. and Mattson, M.P. (1998) Calcium and reactive oxygen species mediate staurosporine-induced mitochondrial dysfunction and apoptosis in PC12 cells. *J. Neurosci. Res.*, **51**, 293–308.

70. Holtzclaw, L.A., Pandhit, S., Bare, D.J., Mignery, G.A. and Russell, J.T. (2002) Astrocytes in adult rat brain express type 2 inositol 1,4,5-trisphosphate receptors. *Glia*, **39**, 69–84.

71. van Es, M.A., Van Vught, P.W., Blauw, H.M., Franke, L., Saris, C.G., Andersen, P.M., Van Den Bosch, L., de Jong, S.W., van 't Slot, R., Birve, A. *et al.* (2007) ITPR2 as a susceptibility gene in sporadic amyotrophic lateral sclerosis: a genome-wide association study. *Lancet Neurol.*, **6**, 869–877.

72. Pedrini, S., Sau, D., Guareschi, S., Bogush, M., Brown, R.H. Jr, Naniche, N., Kia, A., Trotti, D. and Pasinelli, P. (2010) ALS-linked mutant SOD1 damages mitochondria by promoting conformational changes in Bcl-2. *Hum. Mol. Genet.*, **19**, 2974–2986.

73. Scorrano, L., Oakes, S.A., Opferman, J.T., Cheng, E.H., Sorcinelli, M.D., Pozzan, T. and Korsmeyer, S.J. (2003) BAX and BAK regulation of endoplasmic reticulum Ca^{2+}: a control point for apoptosis. *Science*, **300**, 135–139.

74. Cao, G., Pei, W., Ge, H., Liang, Q., Luo, Y., Sharp, F.R., Lu, A., Ran, R., Graham, S.H. and Chen, J. (2002) *In vivo* delivery of a Bcl-X_L fusion protein containing the TAT protein transduction domain protects against ischemic brain injury and neuronal apoptosis. *J. Neurosci.*, **22**, 5423–5431.

75. Chou, S.M. (1995) *Pathology of Motor System Disorder*. Springer, London.

76. Guntinas-Lichius, O., Mockenhaupt, J., Stennert, E. and Neiss, W.F. (1993) Simplified nerve cell counting in the rat brainstem with the physical disector using a drawing-microscope. *J. Microsc.*, **172** (Pt 2), 177–180.

77. Domercq, M., Brambilla, L., Pilati, E., Marchaland, J., Volterra, A. and Bezzi, P. (2006) P2Y1 receptor-evoked glutamate exocytosis from astrocytes: control by tumor necrosis factor-alpha and prostaglandins. *J. Biol. Chem.*, **281**, 30684–30696.

78. Bolte, S. and Cordelieres, F.P. (2006) A guided tour into subcellular colocalization analysis in light microscopy. *J. Microsc.*, **224**, 213–232.